Locally Linear Detail Injection for Pansharpening

JUNMIN LIU[1], YONGCHANG HUI[1], AND PENG ZAN[2]

[1]School of Mathematics and Statistics, Xi'an Jiaotong University, Xi'an 710049, China
[2]Department of Electronic Engineering, University of Maryland at College Park, College Park, MD 20742 USA

Corresponding author: Yongchang Hui (huiyc180@mail.xjtu.edu.cn)

ABSTRACT This paper presents a novel method, referred to as *locally linear detail injection* (LLDI), for the *pansharpening* problem, which is based on the assumption that the spatial details of each *multispectral* (MS) band can be locally and linearly represented by the spatial details of *panchromatic* images. LLDI first exploits such assumption through scales using the *modulation transfer function* (MTF) of the MS instrument and then performs detail injections into the available low-resolution MS images. Visual analysis and quantitative evaluation performed on QuickBird and WorldView-2 data sets at both reduced and full scales show that the proposed LLDI achieves superior improvements over its baselines.

INDEX TERMS Remote sensing, image fusion, pansharpening

I. INTRODUCTION

Many GIS-based applications can benefit from *high-resolution multispectral* (HRM) images. Due to physical constraints, current optical Earth observation satellites, such as QuickBird and WorldView-2, can only produce *high-resolution panchromatic* (HRP) and *low-resolution multispectral* (LRM) images simultaneously over the same areas instead of providing *multispectral* (MS) images with both high spectral and spatial resolutions. In response to the need for HRM images in applications and also by utilizing the complementary characteristics of HRP and LRM images, *pansharpening* [1] has been proposed in the field of remote sensing. As a typical image fusion technique, pansharpening is aimed at integrating the spatial details of a *panchromatic* (PAN) image into the LRM to produce HRM images.

Many pansharpening methods have been developed in past decades, and they can be broadly classified into two main classes: *component substitution* (CS) and *multiresolution analysis* (MRA). Methods of the CS class first transform the LRM image into a new space, totally or partially substitute one component with the histogram matched PAN image, and then apply the inverse transform to obtain the pansharped MS image. Representative methods of this class are *principal component analysis* (PCA) [2] and *intensity-hue-saturation* (IHS) [3]. Although these methods have a relatively good performance in spatial detail enhancement, they may suffer from severe spectral distortion. To address this problem, variants, such as *band-dependent spatial detail* (BDSD) [4], *partial replacement adaptive*

CS (PRACS) [5], and *Gram-Schmidt adaptive* (GSA) [6], have been proposed by considering adaptive weights and injection gains. However, spectral distortion may still occur, especially in some local areas [7].

Methods of the MRA class inject spatial details extracted from the PAN image into the upscaled MS image. Generally, the spatial details are obtained by a multiscale decomposition based on wavelet transformations, low-pass filtering (usually matched to the *modulation transfer function* (MTF) of the sensor), or pyramid decompositions of the PAN image. Some popular methods belonging to this class are *high-pass filtering* (HPF), *smoothing filter-based intensity modulation* (SFIM) [8], the *generalized Laplacian pyramid with context-based decision* (GLP-CBD) [9]. The main advantage of MRA methods is their spectral consistency with the MS image. However, they may be unsatisfactory in terms of spatial enhancement.

CS methods can provide fused results with high geometrical quality of spatial details but with possible spectral distortion, whereas the MRA methods have a superior spectral consistency with the original MS image. To incorporate the advantages of these two classes, researchers have attempted to design some hybrid methods. For example, Liao *et al.* [10] proposed an image fusion framework, called *guided filter PCA* (GFPCA), which applies a guided filter in the PCA domain. Otazu *et al.* [11] proposed the *additive wavelet luminance proportion* (AWLP), which works in the IHS domain by performing MRA of the intensity component. However, it is difficult to obtain a tradeoff relationship between spatial

enhancement and spectral consistency. Both CS and MRA methods are also effective when a multispectral(or hyperspectral) image is the source of high spatial frequency. In that case, the term "pansharpening" is replaced by the term "hypersharpening" [12].

Some methods have been developed that cannot be grouped into the above two classes. These exceptions are based on a Bayesian framework, such as *Bayesian Data Fusion* (BDF) [13], or are inspired by recently developed theories in signal processing such as *sparse representation* (SR) [14] and *total variation* (TV) regularization [15]. They achieve competitive performances with classical CS and MRA methods. However, they are inadequate in practice due to their huge computational complexities and memories. Here, we focus our study on improvements to the CS or MRA methods, which are, in most cases, faster and more efficient than SR- and TV-based methods.

In general, how to model the relationship of the spatial details between the MS and PAN images is crucial to the construction of the HRM images. However, exactly characterizing this relationship is impossible due to the complexity of imaging systems and environments. Considering the solvability of the problem, it is reasonable to assume that there exists a linear relationship characterizing the spatial details between the PAN and MS image in a local region. Based on this assumption, we propose a novel pansharpening method called *locally linear detail injection* (LLDI), in which the missing spatial details of each MS band are estimated by exploiting the local and linear relationships between spatial details of each MS band and the PAN images. In addition, similarly to [4], the local correlation coefficients are estimated at a reduced scale by resorting to the scale invariance assumption. The idea of LLDI is in contrast to traditional works [1] [6], in which the locally or globally linear relationships between PAN and MS band images were employed for the whole original or degraded PAN and MS band images. Thus, the main contribution of this paper is to exploit the locally linear relationships in the frequency domain (or equally between the details of the PAN and MS band images); refer to Section III for more details.

The remainder of this paper is organized as follows. Section II introduces some background about the observation model and the general MRA framework. The proposed LLDI method and experiments are presented in Section III and Section IV. Finally, we draw conclusions in Section V.

II. BACKGROUND

In this paper, images are denoted by bold low-case letters, e.g. $\boldsymbol{x}$, and their elements are denoted with indexes such as $x(i)$. We use $\boldsymbol{x}$ to denote a high resolution image, $\hat{\boldsymbol{y}}$ to denote the spatially blurred version of $\boldsymbol{x}$, and $\boldsymbol{y}$ to denote the blurred and downsampled version of $\boldsymbol{x}$. Image symbols with the superscripts "ms" and "pan," such as $\boldsymbol{x}^{\mathrm{ms}}$ and $\boldsymbol{x}^{\mathrm{pan}}$, denote a multispectral image and a panchromatic image, respectively. The spatial details are denoted by bold low-case letters $\boldsymbol{d}$ and with the subscripts "l" and "h" respectively denoting

the low- and high-resolution versions, e.g. $\boldsymbol{d}_l$ and $\boldsymbol{d}_h$. And symbols i and j indicate the ith and jth pixels, the index k indicates the specific band of the multispectral image.

A. OBSERVATION MODEL

Let $\boldsymbol{x}^{\mathrm{pan}}$ be a PAN image with a high spatial resolution, and let $\boldsymbol{y}_k^{\mathrm{ms}}, k = 1, 2, \cdots, n$, denote n-band MS images with a low spatial resolution over the same area. Pansharpening means combining the PAN and MS images to obtain the MS images $\boldsymbol{x}_k^{\mathrm{ms}}(k = 1, 2, \cdots, n)$ with a spatial resolution as high as that of the PAN image.

The observed low-resolution MS band $\boldsymbol{y}_k^{\mathrm{ms}}$ can be thought of as a blurred and downsampled version of the high-resolution MS band $\boldsymbol{x}_k^{\mathrm{ms}}$

$$\boldsymbol{y}_k^{\mathrm{ms}} = (\boldsymbol{x}_k^{\mathrm{ms}} * f_k) \downarrow r, \quad k = 1, 2, \cdots, n, \qquad (1)$$

where f_k is the blurring filter caused by the optical imaging system for the kth band, $*$ denotes the convolution operator, and $\downarrow r$ refers to downsampling by a factor of r (typically 4). Denote the spatially blurred version of $\boldsymbol{x}_k^{\mathrm{ms}}$, without downsampling, by $\hat{\boldsymbol{y}}_k^{\mathrm{ms}}$, where we have

$$\hat{\boldsymbol{y}}_k^{\mathrm{ms}} = \boldsymbol{x}_k^{\mathrm{ms}} * f_k, \quad k = 1, 2, \cdots, n. \qquad (2)$$

To simplify the estimation, we usually assume that $\hat{\boldsymbol{y}}_k^{\mathrm{ms}}$ can be well approximated by an upsampled one of $\boldsymbol{y}_k^{\mathrm{ms}}$ by interpolation (e.g., bicubic interpolation).

B. THE GENERAL FRAMEWORK

An ideal high-resolution image can be seen as a composition of its low- and high-frequency components. According to (2), the high-resolution MS images can be rewritten as

$$\boldsymbol{x}_k^{\mathrm{ms}} = \hat{\boldsymbol{y}}_k^{\mathrm{ms}} + \boldsymbol{d}_{h,k}^{\mathrm{ms}} \qquad (3)$$

where $\boldsymbol{d}_{h,k}^{\mathrm{ms}} = \boldsymbol{x}_k^{\mathrm{ms}} - \boldsymbol{x}_k^{\mathrm{ms}} * f_k$. Clearly, $\boldsymbol{d}_{h,k}^{\mathrm{ms}}$ are the high-frequency components of the kth HRM band $\boldsymbol{x}_k^{\mathrm{ms}}$. The high-frequency components $\boldsymbol{d}_{h,k}^{\mathrm{ms}}$ are also called the spatial details of $\boldsymbol{x}_k^{\mathrm{ms}}$, as they are the differences between $\boldsymbol{x}_k^{\mathrm{ms}}$ and its spatially degraded version.

With this general model, the key to pansharpening is to infer the spatial details $\boldsymbol{d}_{h,k}^{\mathrm{ms}}$ from the known high-resolution PAN image $\boldsymbol{x}^{\mathrm{pan}}$ and/or low-resolution MS images $\boldsymbol{y}_k^{\mathrm{ms}}$. However, it is extremely ill-posed, as infinitely many $\boldsymbol{d}_{h,k}^{\mathrm{ms}}$ satisfy model (1) and (3). Usually, we assume that the spatial details can be estimated from the weighted high-frequency component of the PAN image as

$$\boldsymbol{d}_{h,k}^{\mathrm{ms}} = g_k(\boldsymbol{x}^{\mathrm{pan}} - \hat{\boldsymbol{y}}^{\mathrm{pan}}), \quad k = 1, 2, \cdots, n, \qquad (4)$$

where g_k is the *injection gain* corresponding to the kth band and $\hat{\boldsymbol{y}}^{\mathrm{pan}}$ is a low-resolution image which corresponds to the low-frequency components of the PAN image.

Different ways of generating the low-resolution approximation of the PAN image yield the pansharpening methods grouped into the CS or MRA classes. For the CS class, it approximates the low-resolution PAN image $\boldsymbol{y}^{\mathrm{pan}}$ as an intensity component $\boldsymbol{I}^{\mathrm{ms}}$, which is a weighted linear combination

of the upsampled MS bands, defined by

$$I^{\mathrm{ms}} = \sum_{k=1}^{n} w_k \hat{y}_k^{\mathrm{ms}}, \tag{5}$$

where $w_k, k = 1, 2, \cdots, n$ are the weights. In contrast to CS-based methods, the MRA class employs spatial filtering of the PAN image to obtain its low-resolution version (with the same size of the PAN image x^{pan}), which is usually band dependent and can be given by

$$\hat{y}_k^{\mathrm{pan}} = x^{\mathrm{pan}} * h_k. \tag{6}$$

where h_k is the low-pass filter of the kth band.

III. LLDI

As mentioned above, the missing high-resolution spatial details $d_{h,k}^{\mathrm{ms}}, k = 1, 2, \cdots, n$, may be inferred from the high-resolution spatial details of the PAN image d_h^{pan} (usually band-dependent $d_{h,k}^{\mathrm{pan}}, k = 1, 2, \cdots, n$). To this end, there are two issues that need to be addressed: 1) how to extract the high-resolution spatial details $d_{h,k}^{\mathrm{pan}}$ from the PAN image such that they are most relevant to the missing spatial details $d_{h,k}^{\mathrm{ms}}$ of the kth MS band and 2) how to model the relationship between the spatial details $d_{h,k}^{\mathrm{ms}}$ and $d_{h,k}^{\mathrm{pan}}$ in a mathematical form that is physically meaningful and readily solvable.

To extract the most relevant spatial details of each MS band from the PAN image, the PAN image should be blurred by the same low-pass filter as each MS band such that the complementary high-pass filter can retain only the spatial details of the corresponding MS band. However, the filter matching of the real MTF of the MS sensor is unknown, and its approximation remains a challenging topic. Fortunately, the sensor gain at the Nyquist frequency is usually provided by the sensor's manufacturer, and thus, the real filter can be reasonably approximated by a *filter matched to the MS sensor's MTF* (referred to as the MTF filter). The effectiveness of the MTF filter has been justified by the BDSD [4] and GLP-CBD [9]. Therefore, we also apply the MTF filter to extract the band-dependent spatial details from the PAN image.

Obviously, the relationship between the spatial details $d_{h,k}^{\mathrm{ms}}$ and $d_{h,k}^{\mathrm{pan}}$ is nonlinear due to the complexity of imaging. However, to be readily solvable and achieve fast implementation, it is common to make a linear approximation of a functional relationship in a local region. Thus, we assume that the spatial details $d_{h,k}^{\mathrm{ms}}$ of the kth MS band can be locally and linearly represented by the spatial details $d_{h,k}^{\mathrm{pan}}$ of the PAN image in a local window. Specifically, in a local window ω_i centered at the ith pixel, the gray values of the kth band spatial details $d_{h,k}^{\mathrm{ms}}$ in the window ω_i can be linearly represented by the corresponding gray values of the spatial details $d_{h,k}^{\mathrm{pan}}$ of the PAN image, i.e., for each pixel $j \in \omega_i$, we have

$$d_{h,k}^{\mathrm{ms}}(j) = a_k(i) d_{h,k}^{\mathrm{pan}}(j) + b_k(i), \tag{7}$$

where $d_{h,k}^{\mathrm{ms}}(j)$ and $d_{h,k}^{\mathrm{pan}}(j)$ are the gray values of the spatial details $d_{h,k}^{\mathrm{ms}}$ and $d_{h,k}^{\mathrm{pan}}$ located at the jth pixel, $a_k(i)$ and $b_k(i)$

are some linear coefficients and constants in the window ω_i for the kth MS band. If both $d_{h,k}^{\mathrm{pan}}$ and $d_{h,k}^{\mathrm{ms}}$ are known, we can determine the linear coefficients by minimizing the following objective function with respect to $a_k(i)$ and $b_k(i)$:

$$\mathcal{O} = \sum_{j \in \omega_i} \left[a_k(i) d_{h,k}^{\mathrm{pan}}(j) + b_k(i) - d_{h,k}^{\mathrm{ms}}(j) \right]^2. \tag{8}$$

Taking its partial gradients yield their optimal solutions as

$$a_k(i) = \frac{\frac{1}{|\omega_i|} \sum_{j \in \omega_i} \xi_{h,k}(j)}{\sigma_{h,k}^{\mathrm{pan}}(i)}, \tag{9}$$

$$b_k(i) = \bar{d}_{h,k}^{\mathrm{pan}}(i) - a_k(i) \bar{d}_{h,k}^{\mathrm{ms}}(j), \tag{10}$$

where

$$\xi_{h,k}(j) = d_{h,k}^{\mathrm{pan}}(j) d_{h,k}^{\mathrm{ms}}(j) - \bar{d}_{h,k}^{\mathrm{pan}}(i) \bar{d}_{h,k}^{\mathrm{ms}}(i), \tag{11}$$

$\bar{d}_{h,k}^{\mathrm{pan}}(i)$ and $\sigma_{h,k}^{\mathrm{pan}}(i)$ are the mean and variance, respectively, of $d_{h,k}^{\mathrm{pan}}$ in ω_i; $\bar{d}_{h,k}^{\mathrm{ms}}(i)$ is the mean of $d_{h,k}^{\mathrm{ms}}$ in ω_i, and $|\omega_i|$ denotes the number of pixels in ω_i. Note that the value of $d_{h,k}^{\mathrm{ms}}(j)$ in model (7) is not identical in all the overlapping windows ω_i that cover the jth pixel. To enforce compatibility, similar to [16], we first average all the possible values of $a_k(i)$ and $b_k(i)$ in the overlapped windows, and then calculate the output by

$$d_{h,k}^{\mathrm{ms}}(j) = \bar{a}_k(j) d_{h,k}^{\mathrm{pan}}(j) + \bar{b}_k(j), \tag{12}$$

where

$$\bar{a}_k(j) = \frac{1}{|\omega_j|} \sum_{i \in \omega_j} a_k(i), \tag{13}$$

and

$$\bar{b}_k(j) = \frac{1}{|\omega_j|} \sum_{i \in \omega_j} b_k(i). \tag{14}$$

However, we can not obtain the local linear coefficients $\bar{a}_k(j)$ and $\bar{b}_k(j)$ at the full scale since the high-resolution spatial details $d_{h,k}^{\mathrm{ms}}$ are unknown and need to be estimated. To estimate the coefficients $\bar{a}_k(j)$ and $\bar{b}_k(j)$, according to the ARSIS concept [17], we resort to the scale invariance assumption [4] [14], i.e. to perform parameter estimation at a reduced scale of the spatial details. The spatial details of the PAN image and the kth MS band at the reduced scale, denoted by $d_{l,k}^{\mathrm{pan}}$ and $d_{l,k}^{\mathrm{ms}}$, respectively, can be obtained by simulating the same degraded process as that of the full-scale counterparts, i.e.,

$$d_{l,k}^{\mathrm{pan}} = \hat{y}_k^{\mathrm{pan}} - ((\hat{y}_k^{\mathrm{pan}} \downarrow r) * f_k) \uparrow r, \tag{15}$$

$$d_{l,k}^{\mathrm{ms}} = \hat{y}_k^{\mathrm{ms}} - (y_k^{\mathrm{ms}} * f_k) \uparrow r. \tag{16}$$

where f_k is the MTF filter of the kth MS band, $\hat{y}_k^{\mathrm{pan}} = x^{\mathrm{pan}} * f_k$, and $\uparrow r$ refers to upsampling by a factor r. Then, we can estimate the coefficients $\bar{a}_k(j)$ and $\bar{b}_k(j)$ by minimizing the objective function $\mathcal{O}$ with the high-resolution spatial details, $d_{h,k}^{\mathrm{pan}}$ and $d_{h,k}^{\mathrm{ms}}$, being replaced by the corresponding low-resolution counterparts, $d_{l,k}^{\mathrm{pan}}$ and $d_{l,k}^{\mathrm{ms}}$, respectively.

Algorithm 1 LLDI

1. **Input:** the high-resolution PAN image x^{pan} and the low-resolution MS images $y_1^{\text{ms}}, y_2^{\text{ms}}, \cdots, y_n^{\text{ms}}$.

2. **Upsampling:** interpolate the MS images into the PAN scale through bicubic interpolation and obtain the interpolated MS images $\hat{y}_1^{\text{ms}}, \hat{y}_2^{\text{ms}}, \cdots, \hat{y}_n^{\text{ms}}$.

- **For** the kth interpolated MS band $\hat{y}_k^{\text{ms}}$ **do**

    3. **Generation of low-resolution PAN image $\hat{y}^{\text{pan}}$ by** filtering the original high resolution PAN image
    $$\hat{y}_k^{\text{pan}} = x_k^{\text{pan}} * f_k, \tag{17}$$
    where f_k is the MTF filter of the kth MS band and x_k^{pan} obtained by the histogram matched to the high-resolution PAN image x^{pan} with the kth MS band.

    4. **Detail extraction of low-resolution $d_{l,k}^{\text{pan}}$ and $d_{l,k}^{\text{ms}}$ by** (15) **and** (16)

    5. **Determination of linear coefficients $a_k(i)$ and $b_k(i)$ by minimizing the following objective function:**
    $$\sum_{j \in \omega_i} \left[a_k(i) d_{l,k}^{\text{pan}}(j) + b_k(i) - d_{l,k}^{\text{ms}}(j) \right]^2. \tag{18}$$

    6. **Reconstruction of high-resolution details of the kth MS band, $d_{h,k}^{\text{ms}}$, by** (12).

    7. **Injection of the details $d_{h,k}^{\text{ms}}$ into $\hat{y}_k^{\text{ms}}$:**
    $$\tilde{x}_k^{\text{ms}} = \hat{y}_k^{\text{ms}} + d_{h,k}^{\text{ms}}. \tag{19}$$

- **End for**

8. **Output:** pansharpened MS images $\tilde{x}_1^{\text{ms}}, \cdots, \tilde{x}_n^{\text{ms}}$.

Based on the above, the procedure of our proposed LLDI method for pansharpening can be summarized as follows.

Some comments on the LLDI algorithm are noteworthy.

- It should be noted that the regression coefficient $a_k(i)$ for the kth MS band seems to be the same as the injection gain $\beta_k(i)$ calculated locally [6] [20]. However, they are different. The regression coefficient $a_k(i)$ is employed in the high-frequency space of the PAN and MS band images in the window ω_i, i.e.,
$$a_k(i) = \frac{\text{cov}(d_{\omega_i}^{\text{ms}}, d_{\omega_i}^{\text{pan}})}{\text{var}(d_{\omega_i}^{\text{pan}})}, \tag{20}$$
where $d_{\omega_i}^{\text{ms}}$ and $d_{\omega_i}^{\text{pan}}$ are the values of the spatial details $d_{h,k}^{\text{ms}}$ and $d_{h,k}^{\text{pan}}$ in the window ω_i, while the injection gain $\beta_k(i)$ exploited such linear relationships in the original pixel value space of the PAN and MS band images, i.e.,
$$\beta(i) = \frac{\text{cov}(y_{\omega_i}^{\text{ms}}, y_{\omega_i}^{\text{pan}})}{\text{var}(y_{\omega_i}^{\text{pan}})} \tag{21}$$
where $y_{\omega_i}^{\text{ms}}$ and $y_{\omega_i}^{\text{pan}}$ are the pixel values of the $y_{h,k}^{\text{ms}}$ and $y_{h,k}^{\text{pan}}$ in the window ω_i. The injection gain $a_k(i)$ is

particularly more effective than the gain setting $\beta_k(i)$ due to the greater variability of high spatial frequencies.

- Similar to the work [4], we also want to "discover" the true detail by exploit the relationship of the high-resolution spatial details through scales. In other words, the high-resolution details $d_{h,k}^{\text{ms}}$ have been reconstructed by locally modeling the linear relationships between the high-resolution details $d_{h,k}^{\text{ms}}$ and $d_{h,k}^{\text{pan}}$, while the estimation of coefficients is performed at a reduced scale. Additionally, the MTFs of the imaging systems are considered when the low-resolution PAN image $\hat{y}_k^{\text{pan}}$ is generated. In this way, the scale invariance assumption holds such that the coefficients $\bar{a}_k(j)$ and $\bar{b}_k(j)$ can be learned at the degraded scale.

- According to the procedure of the LLDI algorithm, we can rewrite the fusion rule of LLDI as
$$\tilde{x}_k^{\text{ms}} = \hat{y}_k^{\text{ms}} + d_{h,k}^{\text{ms}} \tag{22}$$
$$= \hat{y}_k^{\text{ms}} + \bar{a}_k(x_k^{\text{pan}} - \hat{y}_k^{\text{pan}}) + \bar{b}_k \tag{23}$$
where $\bar{a}_k$ and $\bar{b}_k$ are composed of elements of $\bar{a}_k(j)$ and $\bar{b}_k(j)$, respectively. Note that the constant coefficients $\bar{b}_k$ computed in the high spatial frequency domain are expected to be near to zero when the linear regression model is applied on the whole image, since the filtered output of the PAN and MS images have the same mean of the original. However, $\bar{b}_k$ cannot be zero when the linear regression model is applied in a local window. Refer to the experimental results for more detailed analysis. This fusion rule is similar to [6] in that the constant parameters $\bar{b}_k$ are introduced to consider both the spectral gaps between the PAN and MS sensors and the stabilization of the model at different spatial scales. Additionally, the locally linear model for approximating the relationship between the PAN and MS band images can be seen as an approximation of the nonlinear model, as noted in [21].

IV. EXPERIMENTAL RESULTS AND DISCUSSION

In this section, we first apply the proposed LLDI algorithm to two data sets to provide some intuition about how the LLDI model functions, and then, experiments on two other data sets are performed both at reduced and full scales. The fusion results obtained by our proposed LLDI are compared to those of several well-known methods such as BDSD [4], GSA [6], GLP-CA [9] [20], PRACS [5], and the recently proposed nonlinear IHS (NLIHS) method [21].[1] The parameters of each method are manually tuned to achieve the best performance. Note that the LLDI, BDSD, and GLP-CA methods consider the MTF of the MS instrument, and both the GLP-CA and LLDI methods employ the local injection gains but are calculated in different spaces.

---

[1]The codes of all the pansharpening methods have been collected in a MATLAB toolbox, which can be downloaded at http://openremotesensing.net/index.php/codes/11-pansharpening.

(a) PAN   (b) EXP   (c) LLDI   (d) Details

(e) Gains in the frequency space   (f) Gains in the pixel value space   (g) Gains comparison   (h) Constant coefficient
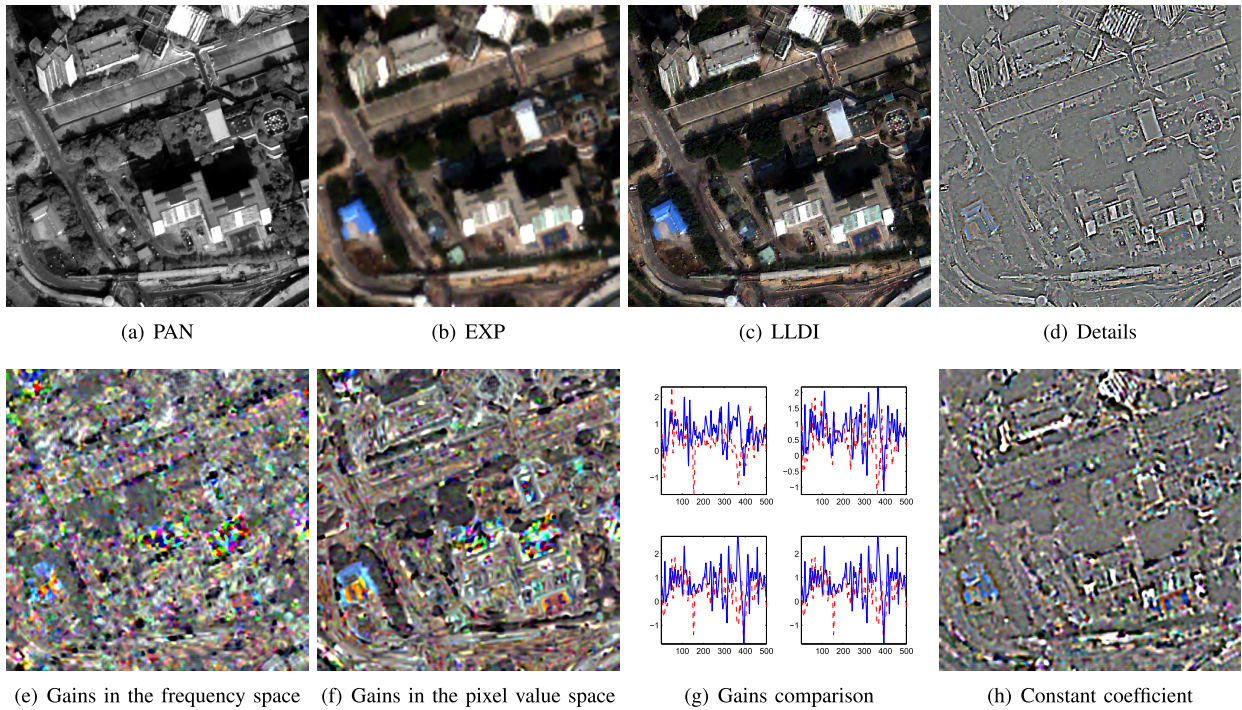
FIGURE 1. The displays of (a) the PAN image, (b) the EXP, (c) the fused image by LLDI, (d) the reconstructed spatial details by LLDI, (e) the injection gains $a_k(i)$ calculated in the frequency space, (f) the injection gains $\beta_k(i)$ in the pixel value space, (g) the gain magnitudes of $a_k(i)$ (red lines) and $\beta_k(i)$ (blue lines) for 100 randomly selected pixels, and (h) the constant coefficients $b_k(i)$ for LLDI.

Four data sets collected by the QuickBird and WorldView-2 satellites have been used for testing and analysis. All the MS images are 128×128 pixels, whereas the corresponding PAN images are 512×512 pixels. The MS image acquired by QuickBird contains four bands, i.e., blue, green, red, and near-infrared (NIR), and its spatial resolution is 2.8 m, while the spatial resolution of the PAN image is 0.7 m. The WorldView-2 satellite can provide a PAN image with a spatial resolution of 2 m and an MS image at a spatial resolution of 0.5 m, where the MS image has eight bands, including 4 traditional bands (red, green, blue, and NIR1 bands) and 4 new bands (coastal, yellow, red edge, and NIR2 bands).

A. TOY EXAMPLES

In this subsection, we apply the LLDI algorithm to two data sets collected by the QuickBird and WorldView-2 satellites to analyze how and why the LLDI model works. The first data set was collected by the QuickBird sensor, where the PAN image is shown in Fig. 1(a), and the original MS image expanded to the scale of the PAN image is reported in Fig. 1(b). In general, the expanded MS image, refereed to as EXP, is assumed as the reference in the visual evaluations. Another data set was collected by the WorldView-2 satellite, and the PAN image and the EXP image are shown in Fig. 2(a) and (b), respectively. It can be observed from these figures that the land-cover types of the two test data sets are mainly buildings (houses and roads) in the QuickBird data

set and vegetated area (trees and grasses) in the WorldView-2 data set.

The fusion results by LLDI are shown in Fig. 1(c) and Fig. 2(c). From these figures, we can find that the proposed LLDI demonstrates an excellent performances in terms of improvement in spatial quality and the preservation of the spectral quality of the original MS images. In addition, the high-resolution spatial details (corresponding to the high-frequency component) $d_{h,k}^{\mathrm{ms}}$, $k = 1, 2, \cdots, n$, for the MS images are properly recovered; refer to the color composites of the high-resolution details reconstructed by LLDI shown in Fig. 1(d) and Fig. 2(d). In addition, Fig. 1(e)-(f) and Fig. 2 (e)-(f) report the injection gains calculated by LLDI in the frequency space, $a_k(i)$, and that calculated in the pixel value space [9] [20], $\beta_k(i)$, respectively. It can be seen from the figures that the inject gains $a_k(i)$ are more unstable than the inject gains $\beta_k(i)$, especially in some dark areas. This may be enrich the variation of the representation of the LLDI. Fig. 1(g) and Fig. 2(g) report the injection gains $a_k(i)$ (red lines) and $\beta_k(i)$ (blue lines) of 100 randomly selected pixels for the red, blue, green and NIR MS bands. We can see that the injection gains $a_k(i)$ and $\beta_k(i)$ follow a similar trend overall but exhibit some subtle and/or large differences for some pixels. The constant coefficients $b_k(i)$ are shown in Fig. 1(h) and Fig. 2(h). The injection gains $a_k(i)$ and the constants coefficients $b_k(i)$ let their locally linear representations, i.e. the reconstructed details as shown in Fig. 1(d) and Fig. 2(d), have the most relevant spatial details of each
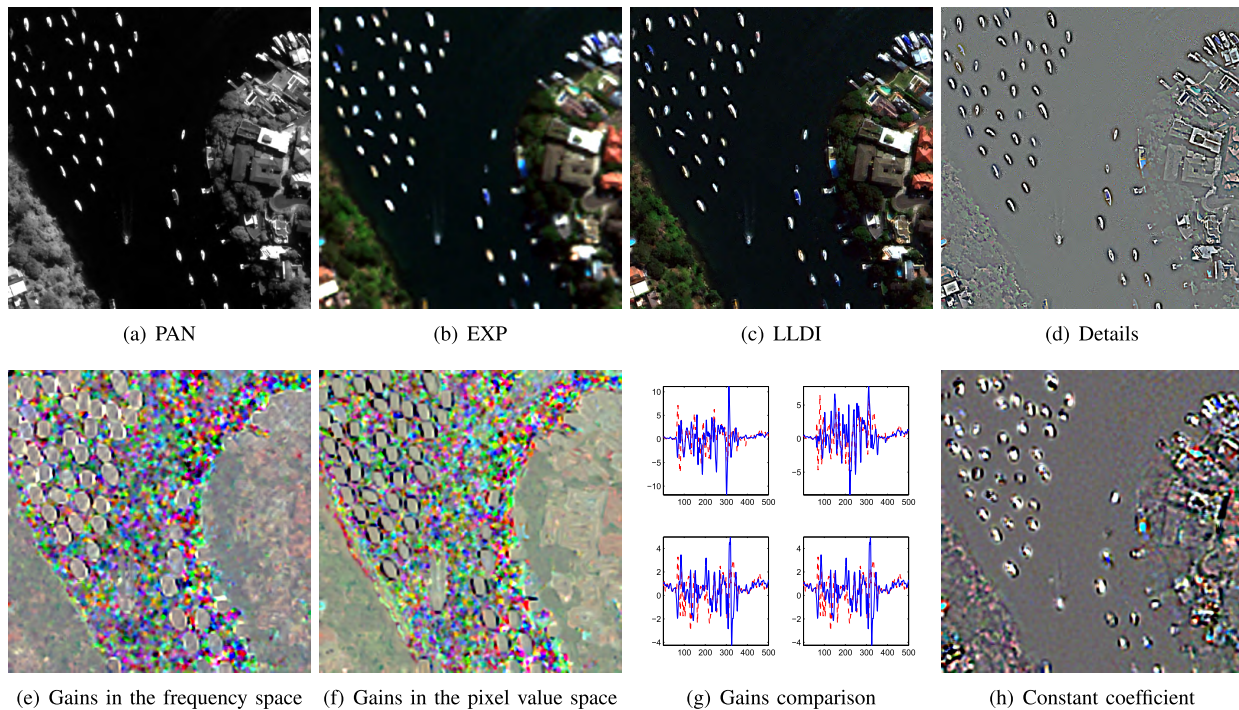
(a) PAN   (b) EXP   (c) LLDI   (d) Details

(e) Gains in the frequency space   (f) Gains in the pixel value space   (g) Gains comparison   (h) Constant coefficient

FIGURE 2. The displays of (a) the PAN image, (b) the EXP, (c) the fused images by LLDI, (d) the reconstructed spatial details by LLDI, (e) the injection gains $a_k(i)$ calculated in the frequency space, (f) the injection gains $\beta_k(i)$ in the pixel value space, (g) the gain magnitudes of $a_k(i)$ (red lines) and $\beta_k(i)$ (blue lines) of 100 randomly selected pixels, and (h) the constant coefficients $b_k(i)$ for LLDI.

TABLE 1. The minimum value (Min.), maximum value (Max.), mean value (Mean), and standard deviations (Std.) of the gains $\beta_k(i)$, $a_k(i)$ and the constant coefficients $b_k(i)$ for different MS bands in the toy example experiments.

		QuickBird				WorldView-2							
		red	green	blue	NIR	red	green	blue	NIR1	coastal	yellow	red edge	NIR2
$\beta_k(i)$	Min.	-10.441	-9.617	-7.334	-21.888	-29.896	-24.323	-24.098	-8.720	-12.759	-6.104	-4.785	-10.612
	Max.	18.415	10.676	8.105	17.726	33.312	29.692	14.168	10.277	11.709	6.829	7.749	8.780
	Std.	0.708	0.613	0.648	1.022	3.489	2.497	1.561	1.251	1.444	0.965	0.878	1.310
	Mean	0.345	0.448	0.485	0.971	0.534	0.474	0.596	0.565	0.428	0.577	0.486	0.597
$a_k(i)$	Min.	-15.478	-6.785	-7.153	-9.322	-28.433	-27.644	-17.553	-10.861	-13.439	-8.199	-9.497	-8.918
	Max.	20.137	8.119	8.656	14.333	31.978	34.501	13.741	8.834	12.892	5.562	7.686	8.789
	Std.	0.734	0.614	0.661	0.842	3.571	2.701	1.724	1.360	1.578	1.045	1.023	1.223
	Mean	0.557	0.666	0.702	1.096	0.383	0.418	0.497	0.504	0.425	0.549	0.508	0.601
$b_k(i)$	Min.	-28.203	-55.164	-49.638	-68.185	-16.157	-26.886	-51.167	-53.013	-54.670	-45.855	-68.749	-68.157
	Max.	27.394	46.566	54.665	59.600	37.174	44.222	66.123	77.962	51.786	76.748	68.082	131.448
	Std.	2.355	4.744	4.702	8.023	1.944	2.777	4.348	4.999	3.666	5.692	7.196	8.033
	Mean	0.004	-0.016	-0.054	0.233	0.182	0.202	0.315	0.464	0.219	0.586	0.535	0.752

MS band extracted from the PAN image. And the minimum value, maximum value, mean value, and standard deviations of the gains $\beta_k(i)$, $a_k(i)$ and the constant coefficients $b_k(i)$ for different MS bands in the experiments are reported in Table 1. From these figures and table, we can further confirm that the differences between the injection gains $a_k(i)$ and $\beta_k(i)$ due to the different ways of calculating, and that the introduction of constant coefficients $b_k(i)$ combined with the injection gains $a_k(i)$ better facilitates the reconstruction of the spatial details and highlight the high-frequency details (such as edges) due to their compensating roles for spectral gaps. In addition, from table 1, it is very interesting to find that the mean values for the constant coefficients $b_k(i)$ are near to zero in

the case of QuickBird, with positive and negative scores for different bands, while the mean values of $b_k(i)$ in the case of WorldView-2 are all positive. This may due to that there are large ocean areas in the WorldView-2 data set and the constant coefficients $b_k(i)$ of the pixels in the ocean areas are positive.

The toy example reveals two interesting points.

- The proposed LLDI method has a good performance both in improving the spatial qualities and in preserving the spectral qualities of the original MS images.
- The injection gains $a_k(i)$ calculated by the spatial details are particularly effective due to the greater variability of high spatial frequencies.
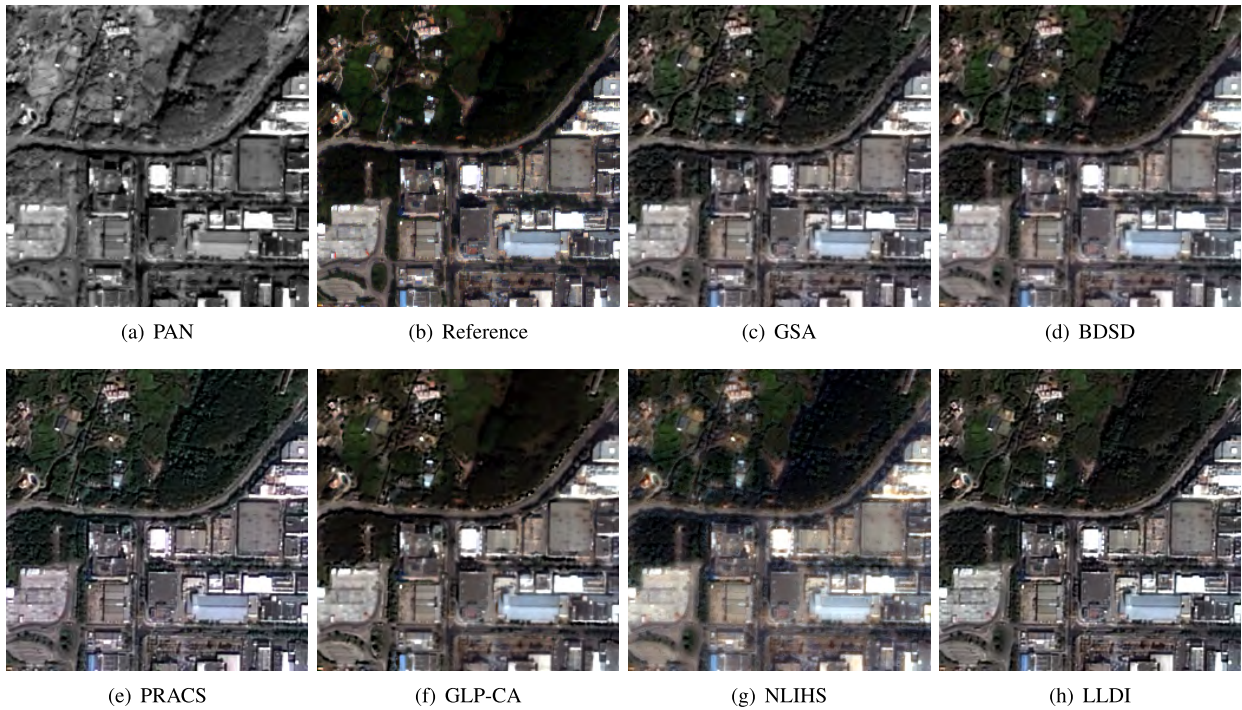
FIGURE 3. The displays of (a) the degraded PAN image, (b) the original MS image (reference), and the fused images obtained by the (c) GSA, (d) BDSD, (e) PRACS, (f) GLP-CA, (g) NLIHS, and (h) LLDI methods for the QuickBird data at reduced scale.

B. EXPERIMENTS AT REDUCED SCALE

In this subsection, experiments are conducted at a reduced scale, i.e., following the protocol of Wald [18] where the original MS and PAN images are first degraded by Gaussian filters, with the gains at the Nyquist frequency being the same as those of the sensors for the MS and PAN images, and by decimating with a factor equal to the resolution ratio. Then, the degraded MS images are sharpened back to the original resolution, and the original MS images are regarded as references. Four reference-based quality indices [1], i.e., the *correlation coefficient* (CC) [22], Q4 [23], the *spectral angle mapper* (SAM) [24], and relative dimensionless global error in synthesis (also called *Erreur Relative Globale Adimensionnelle de Synthése*: ERGAS) [25], have been adopted to quantitatively evaluate the performances of the different methods. The closer the RMSE, SAM, and ERGAS indices are to zeros, the better the pansharpening performances, whereas the closer the CC and Q4 indices are to 1, the higher the qualities. Another two comparison-based quality indices recently proposed in [26], i.e. comparison-based quality (CQ) and comparison-texture-based quality (CTQ), are used to measure the relative quality with two fused images obtained by our LLDI method and another existing one. CQ and CTQ indices have two input images I_1 and I_2 and can indicate the relative quality of image I_1 based on I_2. A positive score of CQ or CTQ means image I_1 is better than the base image I_2 while a negative score of them means the image I_1 is worse than the base image I_2.

1) VISUAL COMPARISON

Fig. 3 shows the degraded PAN image, the original MS image (reference), and the pansharpening results for the QuickBird data set at reduced scale. Except for the degraded PAN image as shown in Fig. 3(a), each display is a composite of the red, blue and green MS bands. By comparing the results obtained by PRACS, as shown in Fig. 3(e), with the reference image, as shown in Fig. 3(b), we can see that spectral distortions are clearly visible in the green areas. Concerning the fusion results of the NLIHS, which is shown in Fig. 3(g), there are also slight spectral distortions, especially for the trees. Although the spectral fidelity of the results of the GSA and BDSD methods, as shown in Fig. 3 (c) and (d), respectively, is impressive, they appear less sharp due to a lack of injection of the spatial details from the PAN image. In this case, as shown in Fig. 3(f) and (h), the results obtained by the GLP-CA and those by our proposed LLDI method can provide visually satisfactory results with respect to the reference MS image due to their performance in recovering local features [20]. Through a visual analysis of the edges of the buildings, we can find that the proposed LLDI method can extract more high-frequency spatial information from the PAN image than can the GLP-CA method.

2) QUANTITATIVE COMPARISON

Table 2 reports the quantitative results of different methods at the reduced scale on the QuickBird and WorldView-2 data sets. Note that the best result for each quality index of the different methods is denoted in bold font. As we can see from the

TABLE 2. Quality indices of different methods at reduced scale.

	QuickBird						WorldView-2					
	GSA	BDSD	PRACS	GLP-CA	NLIHS	LLDI	GSA	BDSD	PRACS	GLP-CA	NLIHS	LLDI
CC	0.950	0.951	0.939	0.953	0.948	**0.954**	0.974	0.977	0.976	0.968	0.939	**0.978**
Q4	0.868	0.869	0.874	0.873	0.807	**0.875**	0.958	0.964	0.965	0.949	0.869	**0.969**
ERGAS	2.156	2.152	2.210	2.194	2.542	**2.148**	3.878	3.581	3.638	4.348	6.878	**3.513**
SAM	2.657	2.638	2.867	2.418	2.806	**2.184**	3.280	3.380	3.869	3.416	5.044	**3.036**

TABLE 3. CQ and CTQ indices at reduced scale with the fused image by LLDI as the base image.

	QuickBird					WorldView-2				
	GSA	BDSD	PRACS	GLP-CA	NLIHS	GSA	BDSD	PRACS	GLP-CA	NLIHS
CQ	-1.338	-1.341	-0.644	-1.134	-3.602	-5.842	-2.465	-6.173	-7.009	-17.028
CTQ	-1.312	-1.295	-0.659	-1.081	-3.188	-7.026	-2.972	-7.061	-8.065	-18.833

(a) PAN   (b) EXP

FIGURE 4. The displays of (a) the PAN image, (b) the original MS image expanded to the size of the PAN image (refereed to as EXP) for the WorldView-2 data.

table, our proposed LLDI method scores the best in terms of all four indices on both data sets. For the QuickBird data set, the PRACS yields much higher values of the Q4 index than do the GSA, BDSD, and NLIHS methods. This can be evidenced from the visual comparisons of spatial details among Figs. 3(d)-(f). When considering the CC and SAM indices, the values of GLP-CA, GSA, and BDSD are close to each other and are better than those obtained by the PRACS and NLIHS methods. The quantitative results confirm the conclusions drawn from the visual analysis. For the WorldView-2 data set, the BDSD, PRACS, and LLDI algorithms achieve similar performances in terms of CC and Q4 values. In addition, our proposed LLDI method achieves a slightly better result compared to the other two methods in terms of the ERGAS index and presents a significant improvement in terms of the SAM index. The CQ and CTQ indices with the image fused by our proposed LLDI method as the base image are reported in Table 3. From this table, we can see that all the CQ and CTQ indices are negative, which means that our results are better than the others.

C. EXPERIMENTS AT FULL SCALE
The quantitative quality assessment of the results at the full scale is difficult because reference high-resolution MS

images are not available. Fortunately, there are indexes that do not need reference images, such as the *quality with no reference* (QNR) [19], which consists of a spectral distortion index D_λ and a spatial distortion index D_s. The closer the D_λ and D_s indices are to zero, the better the pansharpening performances, whereas the closer the QNR index is to 1, the higher the qualities.

1) VISUAL COMPARISON
The high-resolution PAN image and the low-resolution MS images (expanded to the size of the PAN image, refereed to as EXP) collected by the WorldView-2 satellite are shown in Fig. 4(a) and (b). However, it is difficult to visually analyze an image as large 1024×1024 pixels. Therefore, small details, located in the purple rectangle, as shown in Fig. 4(a) and with a size of 200×200 pixels, are shown in Fig. 5 to better facilitate visual inspection. According to this figure, we can find that the BDSD and PRACS methods have a little sharper results than LLDI in some local area such as the grids in the white triangle structures on the left, while they suffer from spectral distortions in the roofs of the buildings and roads (see Fig. 5(d) and (e)) and exist spatial distortion in some other areas, leading to their spatial and spectral indexes worse than the proposed LLDI (see Table 4). Although the GSA and
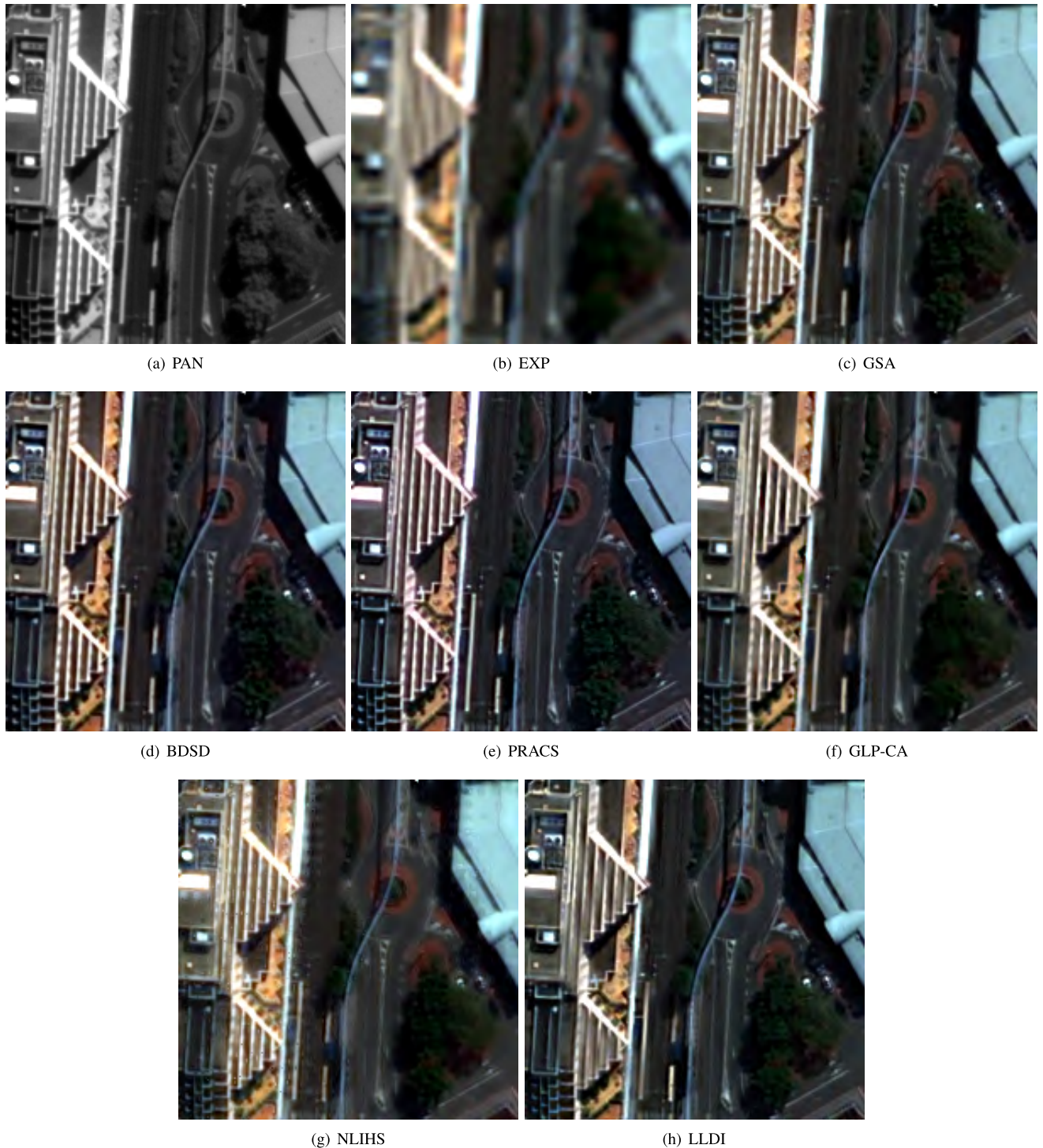
(a) PAN   (b) EXP   (c) GSA

(d) BDSD   (e) PRACS   (f) GLP-CA

(g) NLIHS   (h) LLDI

FIGURE 5. The subset displays of (a) the PAN image, (b) the original MS image expanded to the size of the PAN image (refereed to as EXP), and the fused images obtained by the (c) GSA, (d) BDSD, (e) PRACS, (f) GLP-CA, (g) NLIHS, and (h) LLDI methods for the WorldView-2 data at full scale.

GLP-CA methods achieve high spectral and spatial qualities, some important spatial details are lost when comparing them with our proposed LLDI method. Comparing Fig. 5(c) and (f) with Fig. 5(h) on the edges of the roads and buildings, the results of the GSA and GLP-CA methods are less sharp than are those of our proposed LLDI method.

2) QUANTITATIVE COMPARISON

The objective quality indices of the fusion results at full scale are reported in Table 4. As listed in this table, the proposed LLDI method produces the best results in terms of the spectral distortion index D_λ, the spatial distortion index D_s, and the QNR index among all the compared methods. The NLIHS

TABLE 4. Quality indies of different methods at full scale.

	QuickBird							WorldView-2						
	EXP	GSA	BDSD	PRACS	GLP-CA	NLIHS	LLDI	EXP	GSA	BDSD	PRACS	GLP-CA	NLIHS	LLDI
D_λ	0.000	0.062	0.062	0.060	0.049	0.042	**0.041**	0.000	0.025	0.038	0.048	0.033	0.017	**0.012**
D_s	0.296	0.101	0.080	0.087	0.081	0.105	**0.068**	0.087	0.060	0.028	0.033	0.030	0.056	**0.027**
QNR	0.704	0.843	0.863	0.858	0.874	0.857	**0.894**	0.913	0.917	0.935	0.921	0.938	0.928	**0.961**

TABLE 5. CQ and CTQ indices at full scale with the fused image by LLDI as the base image.

	QuickBird					WorldView-2				
	GSA	BDSD	PRACS	GLP-CA	NLIHS	GSA	BDSD	PRACS	GLP-CA	NLIHS
CQ	-2.168	-2.058	-0.864	-1.051	-3.419	-6.762	-5.475	-1.328	-5.112	-15.648
CTQ	-1.935	-1.886	-0.907	-0.956	-2.811	-7.439	-6.276	-1.551	-5.789	-16.623

method yields comparable results in the preservation of spectral qualities with respect to the LLDI method on both the QuickBird and WorldView-2 data sets. This is in line with the above visual analysis. The low values of the spatial distortion index D_s confirm that the NLIHS method is limited in terms of enhancing the spatial qualities. According to the QNR index, the GLP-CA is slightly worse than our proposed LLDI method, but the former outperforms the other four methods, i.e., GSA, BDSD, PRACS and NLIHS. In terms of the spatial distortion index D_λ in Table 4, the LLDI outperforms the other methods on both data sets. The BDSD and GLP-CA methods perform similarly to each other and slightly better than the PRACS method. And the negative scores of CQ and CTQ, reported in Table 5, also indicate the better performances of LLDI than the others.

V. CONCLUSION

In this paper, a novel method, referred to as locally linear detail injection (LLDI), is proposed for the pansharpening problem. The LLDI method exploits the relationship between the spatial details of the PAN image and those of the MS images, which is formulated as a locally linear model. Based on the scale invariance assumption, the estimation of coefficients is performed at a reduced scale. In contrast to traditional methods, the injection gains are calculated in the frequency space. Due to the greater variability of high spatial frequencies, the proposed LLDI methods are expected to be very effective in extracting the spatial details from the PAN image. The LLDI method is tested on two data sets acquired by QuickBird and WorldView-2 and is compared with several well-known methods. The experimental results demonstrate that our proposed LLDI method can produce results exhibiting promising spectral preservation and satisfactory spatial quality.

ACKNOWLEDGMENT

REFERENCES

[1] G. Vivone, *et al.*, "A critical comparison among pansharpening algorithms," *IEEE Trans. Geosci. Remote Sens.*, vol. 53, no. 5, pp. 2565–2586, May 2015.

[2] P. Chavez and A. Kwateng, "Extracting spectral contrast in landsat thematic mapper image data using selective principal component analysis," *Photogramm. Eng. Remote Sens.*, vol. 55, no. 3, pp. 339–348, 1989.

[3] W. J. Carper, T. M. Lillesand, and R. W. Kiefer, "The use of intensity-hue-saturation transformations for merging SPOT panchromatic and multispectral image data," *Photogram. Eng. Remote Sens.*, vol. 56, no. 4, pp. 459–467, 1990.

[4] A. Garzelli, F. Nencini, and L. Capobianco, "Optimal MMSE pan sharpening of very high resolution multispectral images," *IEEE Trans. Geosci. Remote Sens.*, vol. 46, no. 1, pp. 228–236, Jan. 2008.

[5] J. Choi, K. Yu, and Y. Kim, "A new adaptive component-substitution-based satellite image fusion by using partial replacement," *IEEE Trans. Geosci. Remote Sens.*, vol. 49, no. 1, pp. 295–309, Jan. 2011.

[6] B. Aiazzi, S. Baronti, and M. Selva, "Improving component substitution pansharpening through multivariate regression of MS+Pan data," *IEEE Trans. Geosci. Remote Sens.*, vol. 45, no. 10, pp. 3230–3239, Oct. 2007.

[7] Q. Xu, Y. Zhang, B. Li, and L. Ding, "Pansharpening using regression of classified ms and pan images to reduce color distortion," *IEEE Geosci. Remote Sens. Lett.*, vol. 12, no. 1, pp. 28–32, Jan. 2015.

[8] J. G. Liu, "Smoothing filter based intensity modulation: A spectral preserve image fusion technique for improving spatial details," *Int. J. Remote Sens.*, vol. 21, no. 18, pp. 3461–3472, Dec. 2000.

[9] B. Aiazzi, L. Alparone, S. Baronti, A. Garzelli, and M. Selva, "MTF-tailored multiscale fusion of high-resolution MS and Pan imagery," *Photogramm. Eng. Remote Sens.*, vol. 72, no. 5, pp. 591–596, May 2006.

[10] W. Liao *et al.*, "Processing of multiresolution thermal hyperspectral and digital color data: Outcome of the 2014 IEEE GRSS data fusion contest," *IEEE J. Sel. Topics Appl. Earth Observ. Remote Sens.*, vol. 8, no. 6, pp. 2984–2996, Jun. 2015.

[11] X. Otazu and M. Gonzalez-Audicana, O. Fors, and J. Nunez, "Introduction of sensor spectral response into image fusion methods. Application to wavelet-based methods," *IEEE Trans. Geosci. Remote Sens.*, vol. 43, no. 10, pp. 2376–2385, Oct. 2005.

[12] M. Selva, B. Aiazzi, F. Butera, L. Chiarantini, and S. Baronti, "Hypersharpening: A first approach on SIM-GA data," *IEEE J. Sel. Topics Appl. Earth Observ. Remote Sens.*, vol. 8, no. 6, pp. 3008–3024, Jun. 2015.

[13] D. Fasbender, J. Radoux, and P. Bogaert, "Bayesian data fusion for adaptable image pansharpening," *IEEE Trans. Geosci. Remote Sens.*, vol. 46, no. 6, pp. 1847–1857, Jun. 2008.

[14] M. R. Vicinanza, R. Restaino, G. Vivone, M. D. Mura, and J. Chanussot, "A pansharpeing method based on the sparse representation of injected details," *IEEE Geosci. Remote Sens. Lett.*, vol. 12, no. 1, pp. 180–184, Jan. 2015.

[15] F. Palsson, J. R. Sveinsson, and M. O. Ulfarsson, "A new pansharpening algorithm based on total variation," *IEEE Geosci. Remote Sens. Lett.*, vol. 11, no. 1, pp. 318–322, Jan. 2014.

[16] K. He, J. Sun, and X. Tang, "Guided image filtering," *IEEE Trans. Pattern Anal. Mach. Intell.*, vol. 35, no. 6, pp. 1397–1409, Jun. 2013.

[17] T. Ranchin and L. Wald, "Fusion of high spatail and spectral resolution images: The ARSIS concept and its implementation," *Photogram. Eng. Remote Sens.*, vol. 66, no. 1, pp. 49–61, 2000.

[18] L. Wald, T. Ranchin, and M. Mangolini, "Fusion of satellite images of different spatial resolutions: Assessing the quality of resulting image," *Photogramm. Eng. Remote Sens.*, vol. 63, no. 6, pp. 691–699, Jun. 1997.

[19] L. Alparone *et al.*, "Multispectral and panchromatic data fusion assessment without reference," *Photogramm. Eng. Remote Sens.*, vol. 74, no. 2, pp. 193–200, Feb. 2008.

[20] B. Aiazzi, S. Baronti, F. Lotti, and M. Selva, "A comparison between global and context-adaptive pansharpening of multispectral images," *IEEE Geosci. Remote Sens. Lett.*, vol. 6, no. 2, pp. 302–306, Apr. 2009.

[21] M. Ghahremani and H. Ghassemian, "Nonlinear IHS: A promising method for pan-sharpening," *IEEE Geosci. Remote Sens. Lett.*, vol. 13, no. 11, pp. 1606–1610, Nov. 2016.

[22] L. Alparone *et al.*, "Comparision of pansharpening algorithms: Outcome of the 2006 GRS-S data fusion contest," *IEEE Trans. Geosci. Remote Sens.*, vol. 45, no. 10, pp. 3012–3021, Oct. 2007.

[23] L. Alparone, S. Baronti, A. Garzelli, and F. Nencini, "A global quality measurement of pan-sharpened multispectral imagery," *IEEE Geosci. Remote Sens. Lett.*, vol. 1, no. 4, pp. 313–317, Oct. 2004.

[24] R. H. Yuhas, A. F. H. Goetz, and J. W. Boardman, "Discrimination among semi-arid landscape endmembers using the spectral angle mapper (SAM) algorithm," in *Proc. Summar. 3rd Annu. JPL Airborne Geosci. Workshop*, Pasadena, CA, USA, 1992, pp. 147–149.

[25] L. Wald, "Quality of high resolution synthesised images: Is there a simple criterion?" in *Proc. 3rd Conf. Fusion Earth Data, Merging Point Meas., Raster Maps Remotely Sensed Images*, Sophia Antipolis, France, 2000, pp. 99–103.

[26] H. Liang and D. S. Weller, "Comparison-based image quality assessment for selecting image restoration parameters," *IEEE Trans. Image Process.*, vol. 25, no. 11, pp. 5118–5130, Nov. 2016.

JUNMIN LIU received the Master's degree in computational mathematics from the Ningxia University in 2009 and the Ph.D. degree in applied mathematics from Xi'an Jiaotong University, Xi'an, China, where he is currently an Associate Professor with the School of Mathematics and Statistics. His research interests are focused on hyperspectral unmixing, remotely sensed image fusion, and deep learning.

YONGCHANG HUI received the Ph.D. degree from Northeast Normal University in 2013. He is currently an Assistant Professor with the School of Mathematics and Statistics, Xi'an Jiaotong University, Xi'an, China.

PENG ZAN received the B.S. degree in electrical engineering from Xi'an Jiaotong University, Shaanxi, China in 2014. He is currently pursuing the Ph.D. degree with the University of Maryland at College Park, College Park, MD, USA. His research interests include signal processing and machine learning.

• • •